NACA RM L54C15

NACA

RESEARCH MEMORANDUM

THE AERODYNAMIC CHARACTERISTICS OF TWO SERIES OF LIFTING BODIES AT MACH NUMBER 6.86

By Herbert W. Ridyard

Langley Aeronautical Laboratory
Langley Field, Va.

NATIONAL ADVISORY COMMITTEE
FOR AERONAUTICS

WASHINGTON
May 24, 1954
Declassified February 8, 1960

1W

NACA RM L54C15

NATIONAL ADVISORY COMMITTEE FOR AERONAUTICS

RESEARCH MEMORANDUM

THE AERODYNAMIC CHARACTERISTICS OF TWO SERIES OF LIFTING BODIES AT MACH NUMBER 6.86

By Herbert W. Ridyard

SUMMARY

The results of force tests of two series of lifting bodies in the Langley 11-inch hypersonic tunnel at a Mach number of 6.86 and Reynolds numbers from 1.9×10^6 to 2.6×10^6 based on body length are presented and compared with theory. One series, which consisted of 10° cone cylinders, was tested to investigate the effects of variations in afterbody length on the maximum lift-drag ratio and lift coefficient. The other series, which consisted of drooped-nose, flat-bottomed bodies with D-shaped cross sections, was tested to investigate the effects of fineness ratio, nose shape, and aspect ratio on the maximum lift-drag ratio $(L/D)_{max}$ and on the lift coefficient of D-bodies.

The results obtained by varying the afterbody length of the 10° cone cylinder from 4 to 8 diameters showed that a maximum value of $(L/D)_{max}$ occurred at 6 diameters and that the lift coefficient at $(L/D)_{max}$ decreased as the afterbody length increased.

Drooped-nose, flat-bottomed, D-shaped bodies were found to have higher values of $(L/D)_{max}$ and lift coefficient at $(L/D)_{max}$ than 10° cone cylinders of the same fineness ratio. Further increases in $(L/D)_{max}$ were obtained by modifications of the D-body nose shape and plan form.

The predictions of a combination theory give reasonably good agreement with all the experimental aerodynamic characteristics for the 10° cone cylinders especially at high angles of attack. The Newtonian impact theory gives a similar agreement for the flat-bottomed D-bodies. The cross-flow theory accurately predicts the experimental lift coefficients of the 10° cone cylinders at all but the high angles of attack but underestimates both drag and pitching-moment coefficients. The cross-flow theory predicts that the center-of-pressure locations on the 10° cone cylinders are upstream of the experimental locations.

INTRODUCTION

At hypersonic speeds, relatively blunt bodies have lift coefficients (based on plan-form area) which approach those for wings (see ref. 1); consequently, for a missile configuration a large portion of the lift can be obtained from the body of the missile. The maximum lift-drag ratios of the bodies of reference 1, however, are about half those for the wings. Methods of increasing the maximum lift-drag ratios of hypersonic bodies have been indicated in references 1, 2, and 3. Reference 2 showed that a large increase in the maximum lift-drag ratio of a 20° cone cylinder could be obtained by increasing the afterbody length from 0 to 4 diameters. The use of flat-bottomed bodies, as proposed by Sänger in reference 3 and as indicated experimentally in reference 1, provides another possible means of increasing the maximum lift-drag ratio.

This paper presents the results of an investigation conducted in the Langley 11-inch hypersonic tunnel to evaluate methods of increasing maximum lift-drag ratio. One series of lifting bodies consisted of 10° cone cylinders with afterbody lengths of 4, 6, and 8 diameters. The other series consisted of three drooped-nose, flat-bottomed bodies with D-shaped cross sections subsequently referred to as D-bodies. D-body 1, which had a drooped 10° conical upper nose surface, was tested with afterbody lengths of 4 and 6 diameters. D-body 2, which had a drooped cylindrical upper nose surface, was investigated in an attempt to obtain a lower drag coefficient than that for D-body 1 at the angle of attack for maximum lift-drag ratio. D-body 3 which is similar to, but twice the width of D-body 2, was tested to determine the effect of a change in the aspect ratio of the D-body.

SYMBOLS

α	angle of attack
θ	cone half-apex angle
θ_{eff}	effective cone half-apex angle
δ^*	boundary-layer displacement thickness
d	base diameter of cone-cylinder body and diameter of circle inscribed in D-shaped cross section of base of D-bodies 1 and 2
r_b	radius of base, cone-cylinder body

l_{cone}	length of cone
l	length of model
S_b	model base area
S_p	model plan-form area
S_s	model surface area
L	lift
D	drag
C_L	lift coefficient referred to plan-form area, L/qS_p
C_D	drag coefficient referred to plan-form area, D/qS_p
$C_{D_{\alpha=0}}$	drag coefficient referred to base area for zero angle of attack, D/qS_b
$\left(C_{D_{min}}\right)_p$	minimum drag coefficient based on plan-form area
$\left(C_{D_{min}}\right)_b$	minimum drag coefficient based on base area
D_f	skin-friction drag
C_{D_f}	skin-friction-drag coefficient, D_f/qS_p
C_f	average skin-friction coefficient, Df/qS_s
C_m	pitching-moment coefficient (moments taken about nose of model), Pitching moment$/qS_p l$
$C_{m_\alpha} = \partial C_m/\partial\alpha$	
x_{cp}/l	center-of-pressure location in body lengths from nose
L/D	lift-drag ratio
$(L/D)_{max}$	maximum lift-drag ratio
M	Mach number

TEST APPARATUS AND PROCEDURE

Tunnel

The tests were conducted in the Langley 11-inch hypersonic tunnel at a Mach number of 6.86. A description and calibration of the single-expansion, two-dimensional nozzle used in these tests is given in reference 4.

The stagnation pressure was maintained at about 25 atmospheres and the stagnation temperature was about 700° F. This high stagnation temperature is used to avoid liquefaction of the air in the nozzle. With these conditions, it is possible to maintain flow at a Mach number of about 6.9 in the test region for slightly more than 1 minute. However, warpage of the thin slit-like minimum of the nozzle due to high thermal stresses at this section causes a small but significant variation in Mach number with time. Therefore, data were recorded at a particular time, corresponding to $M = 6.86$, during each operation of this blowdown tunnel. These test conditions correspond to a test Reynolds number of 250,000 per inch.

Models

The basic dimensions of the lifting-body models are shown in figure 1. A photograph of four of the models is shown in figure 2. The original 10° cone cylinder had an afterbody 8 diameters in length which was shortened for subsequent tests to 6 and then 4 diameters. D-body 1 has a drooped 10° conical upper nose surface, flat sides, a flat bottom, and a cylindrical afterbody with a D-shaped cross section which is a semicircle surmounted on a rectangle whose height is half the width. This cross section was chosen by considering the smallest flat-bottomed D-body which could accommodate a cylindrical fuel tank with a diameter equal to that of the 10° cone cylinder. The original D-body 1 had an afterbody 6 diameters in length which was shortened to a length of 4 diameters for subsequent tests. (The diameter is defined for the circle inscribed in the D-shaped cross section.)

D-body 2 consists of a 6-diameter D-shaped afterbody with a modified nose section. The shape of this modified nose corresponds to a length of D-shaped cylinder inclined at an angle of 10° to the flat bottom of the body. The upper-surface elements of the nose are then parallel to the flow when the angle of attack is 10°.

D-body 3 is similar to D-body 2 but is twice the width of D-body 2; the width was increased by including a wedge-slab-shaped portion along the longitudinal center line of the body as shown in figure 1. This modification resulted in an aspect ratio of 0.175 compared to 0.090 for D-body 2.

The cylindrical portions of the 10° cone cylinder and D-body 1 were bored out and supplied with a removable internal plug-rod adaptor (shown in the detailed drawing of the 10° cone cylinder in fig. 1(a)) in order to facilitate the use of either internal or external strain-gage force balances.

A cylindrical unshielded force-balance extension (see fig. 1) was used in the tests of the 10° cone cylinder and D body 1 on the more sensitive normal-force—chord-force balance (to be described later). This extension provided a point at which the balance could be restrained during the interchange of models as a precaution against overloading the balance beams. This precaution was subsequently found to be unnecessary; therefore, the balance extension was not used for the tests of D-bodies 2 and 3. Since the balance extension was not mechanically shielded from the flow, check tests were made on D-body 1 without the balance extension and the results of these check tests agreed within the accuracy of the data with the previous data (taken with the use of the balance extension). This agreement probably occurred because the balance extension in conjunction with the normal-force—chord-force balance was used only at small angles of attack so that the balance extension was shielded in the wake of the model.

Tests

The aerodynamic forces and moments were measured through an angle-of-attack range from 0 to 25° by means of two strain-gage force balances with different sensitivities which were utilized over separate portions of the angle-of-attack range to maintain greater accuracy throughout the test range. For the angles of attack from 0° to 10°, normal and chord forces were measured on an external, sting-mounted, force balance with a capacity of 5 pounds of normal force and 1 pound of chord force. This balance is illustrated in figure 3 of reference 5. For the angle-of-attack range above 10°, lift and drag forces were measured on another external sting-mounted force balance which has capacity loads of 20 pounds of lift and 10 pounds of drag. This balance is shown in figure 2 of reference 5. Pitching moment was measured by means of an internal sting-mounted balance with a capacity of 6 inch-pounds shown in figure 3. Limitations in the movement of the pitch-balance sting support restricted the upper limit of the angle-of-attack range to about 20° for the pitching-moment tests. Schlieren pictures of the models were taken during each tunnel operation and these pictures were used to measure the "run" angles of attack with the aid of an optical comparator.

Model base pressures were measured by means of an orifice located at the nose of the shield of the normal-force—chord-force balance. The base pressures were used to estimate the base drags and then the body drags measured by the force tests were corrected to the condition of

free-stream pressure acting on the base of the models. The base-pressure measurements were restricted to the angle-of-attack range from 0° to 10° since this was the operating range for the normal-force—chord-force balance. The estimated values of the base drags above 10° angle of attack were very small compared to the forebody drags; in fact, above 15° angle of attack no correction was made for base drag.

Accuracy of the Data

The important sources of error in the test data arise from measurements of Mach number, pressures, aerodynamic forces, and angles of attack. Upon consideration of these sources of error it is estimated that the probable maximum errors in the force coefficients, taken as averages for all the test models, vary from about ±5 percent at very small angles of attack to about ±2 percent at medium and high angles of attack. The angles of attack are accurate to within ±0.1°.

THEORETICAL METHODS

Pressures on 10° Cone Cylinder

The theoretical analysis for the 10° cone cylinder was performed by two methods. The first method was a combination of cone and Newtonian impact theory. The second method was cross-flow theory.

Combination of cone and Newtonian impact theories.- No single theory predicts accurately the forces on 10° cone cylinders at angles of attack in hypersonic flow. Examination of available theoretical work, however, has led to a method which gives reasonable results. In this method, cone and Newtonian impact theories are applied to the various portions of the angle-of-attack range according to the applicability of these theories.

At zero angle of attack, only the pressures on the cone need be considered and an initial solution for the nonviscous forces was obtained from the tabulated results of reference 6 which have been calculated from the exact relations of Taylor and Maccoll (ref. 7). An iterated solution for the cone at $\alpha = 0°$ was obtained from reference 6 by use of an effective cone angle which takes account of the displacement of the potential flow by the boundary layer. This effective cone angle will be discussed further under the heading "Skin-Friction Drag."

For small angles of attack (0° to 5°) the forces on the cone were obtained from the tabulated coefficients for inclined cones presented in reference 8 which have been calculated by the second-order theory of Stone (ref. 9). The forces on the cylinder were determined separately

by means of the Newtonian impact theory according to reference 10 for the case where centrifugal forces are neglected. The application of the impact theory was simplified by assuming that free-stream pressure existed on the leeward side of the cylinder. As long as this assumed pressure is taken as free stream or less, its magnitude will be small in comparison to the pressures on the windward side of the body at the test Mach number.

For the larger angles of attack ($\alpha > 5^\circ$), the theoretical nonviscous forces were found by applying Newtonian impact theory to the entire configuration.

This analysis of the nonviscous air forces on the 10° cone cylinder using a combination of theories depending on the angle-of-attack range will be referred to as the combination theory in the remainder of this paper.

The results of the cone theory, which was used as a part of the combination theory, were compared with the results of linearized cone theory obtained by use of reference 11. For zero angle of attack the results from linearized theory were identical to those from the exact method (ref. 6). For small angles of attack the results of the linearized theory gave poor agreement with those for inclined cones presented in reference 8, a result which was expected since the cone half-apex angle is nearly as great as the Mach angle of the flow at Mach number 6.86.

Cross-flow theory.- The theoretical forces on the 10° cone cylinder were also calculated by Allen's cross-flow theory (see ref. 12). This solution considers viscous cross-flow effects as well as potential pressure forces and requires a determination of drag at zero lift. Wherever the cross-flow theory is presented in this paper, the theoretical values include the measured drag at zero lift. The application of this theory throughout the angle-of-attack range of these tests required the use of a correlation of cross-drag coefficient with cross Mach number as presented in references 13 or 14.

Pressures on D-Body

The nonviscous forces on the D-bodies were calculated with the aid of the general method for the application of the Newtonian impact theory presented in reference 15. In the application of the theory, the centrifugal forces were neglected and it was assumed that free-stream pressure exists on the leeward side of the body.

Skin-Friction Drag

The skin-friction drag for the lifting bodies at zero angle of attack was determined on the assumption that the boundary layer was laminar. This assumption was based on the appearance of the boundary layer on schlieren photographs of the bodies and recent unpublished boundary-layer velocity-profile measurements on a hollow cylindrical tube in the Langley 11-inch hypersonic tunnel at $M = 6.9$. On the schlieren photographs, the boundary layer appears to be sharply defined, which is an indication of the high-density gradients near the outer edge of a laminar boundary layer. Furthermore, there is no indication of transition of the boundary layer from laminar to turbulent. For the lifting bodies, however, these photographic evidences are not as conclusive as they would be for two-dimensional bodies. Velocity-profile measurements on the hollow cylindrical tube indicated that boundary-layer transition occurred at Reynolds numbers between 8×10^6 and 9×10^6, values which are much greater than the Reynolds numbers of the lifting bodies (1.9×10^6 to 2.6×10^6).

Three different methods (refs. 16, 17, and 18) which contain various degrees of simplification in their derivation and application were used to calculate the skin-friction drag for the 10° cone cylinders at zero angle of attack.

In computing skin-friction drag at $\alpha = 0^\circ$ for the D-bodies, the values for the 10° cone-cylinder bodies with corresponding lengths were multiplied by the ratio of the surface areas, that is

$$D_{f_{\text{D-body}}} = D_{f_{\text{cone-cylinder}}} \frac{(S_s)_{\text{D-body}}}{(S_s)_{\text{cone-cylinder}}}$$

The skin-friction drag determined for $\alpha = 0^\circ$ was added to the nonviscous drag throughout the angle-of-attack range as an approximation to the viscous drag at angles of attack.

Application of the method of Von Kármán and Tsien.- Von Kármán and Tsien in reference 16 solved the boundary-layer momentum equation for steady, compressible, laminar flow over a flat plate. For $M = 6.86$, reference 16 gives the flat-plate skin-friction coefficient for no heat transfer as $C_f\sqrt{R} = 1.05$. The skin-friction-drag coefficient was then based on the body plan-form area.

Application of the method of Bertram.- A more detailed computation of the boundary layer and skin friction on the 10° cone cylinder at $\alpha = 0^\circ$ was performed with the aid of reference 17 which contains

Bertram's solution of the compressible boundary-layer equations for steady flow over a flat plate with the assumption of a linear velocity profile.

To compute the skin friction for the 10° cone, Mangler's transformation (ref. 19) was used to convert the flat-plate skin-friction equation of reference 17 to an equivalent relation for a cone. An initial value of C_{D_f} was found by substituting the theoretical potential flow quantities at the surface of a 10° cone (as obtained from ref. 6) into the transformed skin-friction equation. This initial result was iterated to determine the effect on the pressure and skin-friction drag caused by the displacement of the potential flow by the boundary layer in the following manner. First, the boundary-layer displacement thickness at the cone-cylinder juncture was calculated for the initial conditions by use of the displacement-thickness relation of reference 17 which was transformed to the equivalent relation for a cone. This value of δ^* was added to the radius at the base of the cone and this new radius was used to define an effective cone, that is, the variation of δ^* along an element of the cone was assumed linear and the effective cone formed by the addition of the boundary-layer displacement thickness to the cone radius gives an effective half-cone angle,

$$\theta_{eff} = \tan^{-1} \frac{r_b + \delta^* \sec \theta}{l_{cone}}$$

or for small angles, $\theta_{eff} = \tan^{-1} \left(\frac{r_b + \delta^*}{l_{cone}} \right)$. The iterated value of C_{D_f} was then obtained from the transformed skin-friction equation by use of the theoretical potential flow quantities (obtained from ref. 6) at the surface of the effective cone. An iterated value of the theoretical nonviscous force on the cone was also obtained from reference 6 by use of the effective cone angle.

The skin-friction drag on the cylindrical afterbody was found by a direct application of the flat-plate results of reference 17. To perform this calculation, three assumptions were made as follows: (1) an instantaneous two-dimensional expansion occurred at the cone-cylinder juncture; (2) the integrated boundary-layer momentum loss was assumed to be constant across this pressure drop, and (3) the Mach number variation along the surface of the cylinder was assumed small and taken to be zero. In the light of these assumptions, an equivalent length of flat plate was calculated that would give the same integrated momentum loss as that which was obtained from the cone boundary-layer calculation at the cone-cylinder juncture. The skin-friction drag on the cylinder was then determined by considering that the initial boundary-layer growth takes place over a cylinder of length equal to the equivalent flat plate. The calculation

was performed for two separate constant Mach numbers as prescribed by assumption 3. The first Mach number was 7.25, the theoretical value immediately behind the sudden expansion, and the second was 6.86, the free-stream Mach number. An average value of the skin-friction-drag coefficients for these two Mach numbers was considered a good approximation to the actual case in which the Mach number varies along the cylinder asymptotically approaching the free-stream value.

Application of the method of Rott and Crabtree.- The skin-friction-drag equations of Rott and Crabtree (ref. 18) are somewhat more rigorous than those of reference 17. A fourth-order polynomial is used for the velocity profile; however, the usual Pohlhausen parameters have been modified according to Thwaites (ref. 20). In addition, the equations of reference 18 were applied with a theoretically more rigorous assumption as to the Mach number distribution along the cylinder, that is, the Mach number was assumed to vary parabolically from $M = 7.25$ at the cone-cylinder juncture and to approach $M = 6.86$ asymptotically. This parabolic variation was extrapolated from a theoretical Mach number distribution determined by the method of characteristics for a 10° cone-cylinder body of revolution at a Mach number of 7. The form of the Mach number distribution over the cylinder seems to make little difference in the resulting friction drag since reference 18 was also applied to the cylinder with the assumption of a linear variation of Mach number with distance and then with the assumption of a constant Mach number over the cylinder with only about a 1 to 2 percent change in the skin-friction drag.

PRESENTATION OF RESULTS

The aerodynamic coefficients presented in this paper are, in general, based on body plan-form area except where otherwise noted.

The variation with angles of attack of the experimental force coefficients, C_L, C_D, and L/D for the 10° cone cylinders with afterbody lengths of 4, 6, and 8 diameters are presented in figure 4. For comparison with the experimental data, theoretical predictions of the force coefficients are also presented in this figure. The solid curves represent the combination theory and the dashed curves represent the cross-flow theory, both described previously under the heading of "Theoretical Methods." The theoretical skin-friction drag as found with the aid of reference 17 was included in the determination of the combination-theory drag coefficients.

The variations with angle of attack of the experimental force coefficients C_L, C_D, and L/D for D-bodies 1, 2, and 3 are presented in

figures 5, 6, and 7, respectively. On the same figures the experimental data are compared with the results predicted by the Newtonian impact theory (ref. 15). Theoretical skin-friction drag adapted from the application of reference 17 to the 10° cone cylinders is included in the determination of the theoretical drag coefficients.

Typical schlieren pictures of the lifting bodies at various angles of attack at $M = 6.86$ are shown in figure 8.

The variations with afterbody length of the maximum lift-drag ratios and the lift and drag at the angle of attack at which $(L/D)_{max}$ occurs for the lifting bodies as taken from figures 4-7 are presented in figure 9. The maximum lift-drag ratios for the 20° cone cylinders of reference 2 are also included in figure 9 for comparison purposes.

A comparison of the theoretical drag coefficients based on base area at zero angle of attack with the experimental values for the 10° cone cylinder over the range of afterbody lengths are presented in figure 10. Both the theoretical inviscid and viscid parts of the drag are shown in this figure.

The variations of the pitching-moment coefficients referred to the nose and the center-of-pressure locations in body lengths measured from the nose with angle of attack for the 10° cone cylinders and D-bodies 1 are presented in figures 11 and 12. Theoretical pitching moment and center-of-pressure locations predicted by Newtonian impact theory appear as solid curves in figures 11 and 12 and the cross-flow theory appears as dashed curves in figure 11.

DISCUSSION OF RESULTS

Lifting-Body Force Coefficients

The experimental force coefficients C_L and C_D of the 10° cone cylinders (fig. 4) are underestimated somewhat by the prediction of the combination theory at low angles of attack ($0° \leq \alpha \leq 5°$). These predictions, however, are better than they would have been if the Newtonian theory had been applied to the whole configuration at low angles of attack. At higher angles of attack ($\alpha > 5°$) the results of Newtonian impact theory show good agreement with the experimental lift and drag coefficients. The cross-flow theory gives a good estimate of the lift coefficients of the 10° cone cylinders throughout most of the angle-of-attack range but overestimates C_L at high angles of attack. Cross-flow-theory results underestimate the experimental drag coefficients at angles of attack.

The values of L/D predicted by the combination theory agree with the experimental values of (L/D) (fig. 4) at the small and large angles of attack but the experimental values of $(L/D)_{max}$ are overestimated by as much as 10 percent. The cross-flow-theory results agree with the experimental values of (L/D) only at small angles of attack; the experimental values of $(L/D)_{max}$ are overestimated by as much as 50 percent.

The experimental force coefficients C_L and C_D of the D-bodies (figs. 5, 6, and 7) are underestimated somewhat by the Newtonian impact theory with better agreement occurring at the high angles of attack. In the case of L/D, the results of Newtonian impact theory overestimate the experimental data at low angles of attack with better agreement occurring at high angles of attack.

The varying degrees of agreement between experiment and the Newtonian impact theory over the angle-of-attack range can be understood better with the aid of the schlieren pictures of the lifting bodies shown in figure 8. The Newtonian impact theory assumes that the shock wave lies along the windward surface of the body. As can be seen in figure 8 the shock waves are highly swept at M = 6.86 for all the lifting bodies and become more nearly parallel to the body surfaces as the angle of attack is increased, indicating that Newtonian impact theory and experiment should agree more closely as the angles of attack are increased.

The lifting-body minimum-drag-coefficient values are somewhat obscure in figures 4 to 7; therefore, they are presented, based on body plan-form area, in the following table along with the minimum drag coefficients based on base area and the angles of attack at which the values of $C_{D_{min}}$ occur.

Body	Afterbody length, diam.	Angle of attack for $C_{D_{min}}$, deg	$(C_{D_{min}})_p$	$(C_{D_{min}})_b$
10° cone cylinder	4	0	0.0072	0.063
	6	0	.0063	.071
	8	0	.0055	.077
D-body 1	4	3	.0098	.075
	6	3	.0090	.089
D-body 2	6	3.5	.0068	.085
D-body 3	6	3.5	.0072	.087

It is seen from this table that $C_{D_{min}}$ based on body plan-form area decreases with increasing afterbody length while $C_{D_{min}}$ based on the more usual reference area for bodies, base area, increases with increasing afterbody length. The values of $C_{D_{min}}$ based on either reference area are smaller for D-bodies 2 and 3 than for D-body 1 with the same afterbody length.

Comparison of the Lifting-Body Force Coefficients at $(L/D)_{max}$

The variations with afterbody length of the maximum lift-drag ratios and the lift and drag at $(L/D)_{max}$ for the lifting bodies (fig. 9) shows that the values of $(L/D)_{max}$ for the 10° cone cylinder attained a maximum of 3.2 at an afterbody length of about 6 diameters. Both C_L and C_D at maximum lift-drag ratio decrease slightly with afterbody length.

The dashed-line extrapolations of the variations of $(L/D)_{max}$ with afterbody length for the 20° cone-cylinder bodies of revolution of reference 2 and the 10° cone-cylinder bodies of revolution of this paper indicate that by decreasing the cone angle large increases in $(L/D)_{max}$ are obtained.

The experimental variation of $(L/D)_{max}$ with afterbody length for D-body 1 shows about a 7-percent increase in $(L/D)_{max}$ as the afterbody is increased from 4 to 6 diameters. In every case tested, D-body 1 exhibits higher values of $(L/D)_{max}$ as well as lift coefficients than any of the 10° cone cylinders. Therefore, for the fineness-ratio range tested, a D-body with the same fineness ratio as a 10° cone-cylinder body of revolution has significantly higher values of $(L/D)_{max}$ and lift coefficient at $(L/D)_{max}$. These gains associated with D-body 1 are obtained at the expense of higher minimum drags; for example, as shown in the preceding table, D-body 1 with the 6-diameter afterbody length has a minimum drag coefficient based on body plan-form area of 0.0090 compared to 0.0063 for the 10° cone cylinder of the same length. However, for missiles which are to operate near the angle of attack for $(L/D)_{max}$, the minimum drags are not usually important.

According to figure 9, D-body 2 shows an 11-percent increase in $(L/D)_{max}$ above that of the D-body 1 with the same afterbody length. This increase in $(L/D)_{max}$ resulted from the use of a modified nose whose upper surface is cylindrical and parallel to the free stream at $\alpha = 10°$, the angle at which $(L/D)_{max}$ occurs for all the D-bodies.

D-body 3, which has a nose section similar to that of D-body 2 and is twice the width of D-body 2, shows a 10-percent increase in $(L/D)_{max}$ above that of D-body 2, a result that indicates the desirability of increasing the plan-form aspect ratio of flat-bottomed bodies. The combination of alterations to the 10° cone cylinder, that is, flattening the bottom, modifying the nose shape, and increasing the aspect ratio results in D-body 3 having an $(L/D)_{max}$ which is 37 percent higher than the highest $(L/D)_{max}$ for the 10° cone cylinders.

Preliminary evidence of the effect of aspect ratio on flat-bottomed bodies had been obtained from tests of several thin "plan-form" models in the Langley 11-inch hypersonic tunnel. These plan-form models were designed with various aspect ratios and plan-form shapes similar to those of the D-bodies, but they were designed with thin wedge-shaped profiles to "shield" the upper surfaces from the flow above about $\alpha = 3°$. The results of these tests showed a trend of increasing $(L/D)_{max}$ with aspect ratio; however, the detailed results of these tests were not considered sufficiently accurate to be presented in this paper.

Skin-Friction Drag

The results of the theoretical calculations of skin-friction drag on the 10° cone cylinders are indicated in figure 10 which includes both the inviscid and viscid parts of the theoretical minimum drag. As shown in this figure, the experimental minimum drag coefficients based on base area for the 10° cone cylinders are underestimated by all of the theories; however, the results of the iterated theoretical viscid drag determined by references 6 and 17 give the best prediction of the experimental data. The iterated values of the skin-friction drag found by use of references 6 and 17 were therefore used in the determination of the theroetical drag curves presented as combination theory in figure 4 and as Newtonian impact theory in figures 5 to 7. As indicated by the slope of the variation of the experimental drag coefficients with afterbody length and the dashed-line extrapolation of these data, it appears that the theories used give a better prediction of the cone drag than of the cylinder drag. It is interesting to note that the iterated inviscid cone drag is almost 25 percent greater than the initial estimate of the inviscid cone drag because of the distortion of the cone profile by the displacing effect of the boundary layer. This increase in the inviscid drag is not entirely reflected in the total theoretical drag because the skin-friction drag is somewhat lower for the distorted cone.

Lifting-Body Stability Parameters

The experimental variations of pitching-moment coefficient (moments taken about the nose) with angle of attack for the 10° cone cylinders

with the 4-, 6-, and 8-diameter afterbodies are given in figure 11. Most evident is the increasing rate of change of pitching moment with angle of attack; for example, C_{m_α} at $\alpha = 20^\circ$ is about five times C_{m_α} at $\alpha = 0^\circ$. This nonlinearity is predicted by the combination theory; however, this theory underestimates the experimental values for all 10° cone cylinders at low angles of attack. Better agreement occurs as the angles of attack are increased.

The center-of-pressure locations (in body lengths from the nose) for the 10° cone cylinders (fig. 11) show about a 5- to 10-percent movement toward the rear of the bodies as the angle of attack is increased. This rearward variation in center of pressure with angle of attack is predicted by the combination theory and the agreement between experiment and the combination theory is good at high angles of attack. There is also a small movement of the center of pressure toward the nose of the 10° cone cylinder with increasing afterbody length. This trend is predicted by both the combination and the cross-flow theory; however, the cross-flow theory predicts a more forward location of the center of pressure throughout the angle-of-attack range. The experimental centers of pressure are located at about 50 percent of the body length for $\alpha = 8^\circ$, the angle of attack at which $(L/D)_{max}$ occurs for the 10° cone cylinders.

The experimental variations of C_m with α for D-bodies 1 given in figure 12 are also nonlinear; for example, C_{m_α} at $\alpha = 20^\circ$ is about four times C_{m_α} at $\alpha = 0^\circ$. The Newtonian impact theory predicts this nonlinearity and gives good agreement with experiment at high angles of attack. At low angles of attack the theory underestimates the experimental pitching-moment coefficients. The almost negligible change in experimental C_m with afterbody length for a particular angle of attack is predicted by the Newtonian impact theory.

The center-of-pressure location on D-body 1 is about 60 percent of the body length from the nose for most of the angle-of-attack range as shown both experimentally and theoretically in figure 12. Between 0° and 5°, however, there are large variations in center-of-pressure location with α; in fact, the experimental center-of-pressure variation with α becomes discontinuous at about 2.2°, the angle of attack for zero lift. This discontinuity is due to the unsymmetrical profile of the D-body. The Newtonian impact theory predicts the occurrence of this discontinuity at about $\alpha = 3.5^\circ$. This discrepancy is due to the inability of the Newtonian theory to predict accurately the angle of zero lift. The variation in center-of-pressure location with afterbody length for a particular angle of attack is negligible as predicted by the theory.

Since the variations of center-of-pressure location with α for both the 10° cone cylinders and D-body 1 are generally small, the

nonlinear variations of C_m with α can be attributed to the nonlinear variations of C_L and C_D with α.

SUMMARY OF RESULTS

The primary results of the lifting-body tests at Mach number 6.86 may be summarized as follows:

1. The results obtained by varying the afterbody length of the 10° cone cylinder from 4 to 8 diameters showed that a maximum value of the maximum lift-drag ratio $(L/D)_{max}$ occurred at 6 diameters and that the lift coefficient at $(L/D)_{max}$ decreased as the afterbody length increased.

2. Flat-bottomed D-shaped bodies with 10° drooped conical upper nose surfaces were found to have higher values of $(L/D)_{max}$ and lift coefficient at $(L/D)_{max}$ than 10° cone cylinders of the same fineness ratio.

3. The use of a D-body nose shape whose upper surface was cylindrical and parallel to the free-stream flow at $(L/D)_{max}$ resulted in improved lift and drag characteristics as compared to the drooped conical nose. Further improvement in the D-body $(L/D)_{max}$ and lift coefficient were obtained by increasing the aspect ratio of the plan form.

4. The rate of change of pitching-moment coefficient with angle of attack increased with angle of attack but the pitching-moment coefficient did not vary appreciably with afterbody length at a given angle of attack for either the 10° cone cylinders or the drooped-conical-nose D-bodies.

5. The center-of-pressure locations on the 10° cone cylinders move rearward about 5 to 10 percent with increasing angle of attack. The center-of-pressure location on the drooped-conical-nose D-body is independent of angle of attack α above $\alpha = 5°$; below $\alpha = 5°$, there is a discontinuous variation in center-of-pressure location with angle of attack due to the unsymmetrical profile of the D-body. The center-of-pressure location does not vary appreciably with afterbody length for either the 10° cone cylinders or the D-bodies.

6. The predictions of a combination theory give reasonably good agreement with all the experimental aerodynamic characteristics for the 10° cone cylinders especially at high angles of attack. The Newtonian impact theory gives a similar agreement for the flat-bottomed D-bodies.

The cross-flow theory accurately predicts the experimental lift coefficients of the 10° cone cylinders at all but the high angles of attack but underestimates both drag and pitching-moment coefficients. The cross-flow theory predicts that the center-of-pressure locations on the 10° cone cylinders are upstream of the experimental locations.

7. The experimental minimum drag coefficients for the 10° cone cylinders are underestimated by the theoretical analysis.

Langley Aeronautical Laboratory,
National Advisory Committee for Aeronautics,
Langley Field, Va., March 2, 1954.

REFERENCES

1. McLellan, Charles H.: Exploratory Wind-Tunnel Investigation of Wings and Bodies at M = 6.9. Jour. Aero. Sci., vol. 18, no. 10, Oct. 1951, pp. 641-648.

2. Cooper, Ralph D., and Robinson, Raymond A.: An Investigation of the Aerodynamic Characteristics of a Series of Cone-Cylinder Configurations at a Mach Number of 6.86. NACA RM L51J09, 1951.

3. Sänger, E., and Bredt, J.: A Rocket Drive for Long Range Bombers. Translation CGD-32, Tech. Information Branch, Bur. Aero., Navy Dept., Aug. 1944.

4. McLellan, Charles H., Williams, Thomas W., and Beckwith, Ivan E.: Investigation of the Flow Through a Single-Stage Two-Dimensional Nozzle in the Langley 11-Inch Hypersonic Tunnel. NACA TN 2223, 1950.

5. McLellan, Charles H., Bertram, Mitchel H., and Moore, John A.: An Investigation of Four Wings of Square Plan Form at a Mach Number of 6.86 in the Langley 11-Inch Hypersonic Tunnel. NACA RM L51D17, 1951.

6. Staff of the Computing Section, Center of Analysis (Under Direction of Zdeněk Kopal): Tables of Supersonic Flow Around Cones. Tech. Rep. no. 1, M.I.T., 1947.

7. Taylor, G. I., and Maccoll, J. W.: The Air Pressure on a Cone Moving at High Speeds. Proc. Roy. Soc. (London), ser. A., vol. 139, no. 838, Feb. 1, 1933, pp. 278-311.

8. Staff of the Computing Section, Center of Analysis (Under Direction of Zdeněk Kopal): Tables of Supersonic Flow Around Cones of Large Yaw. Tech. Rep. no. 5, M.I.T., 1949.

9. Stone, A. H.: On Supersonic Flow Past a Slightly Yawing Cone. II. Jour. Math. and Phys., vol. XXX, no. 4, Jan. 1952, pp. 200-213.

10. Grimminger, G., Williams, E. P., and Young, G. B. W.: Lift on Inclined Bodies of Revolution in Hypersonic Flow. Jour. Aero. Sci., vol. 17, no. 11, Nov. 1950, pp. 675-690.

11. Ferri, Antonio: Elements of Aerodynamics of Supersonic Flows. The MacMillan Co., 1949.

12. Allen, H. Julian: Estimation of the Forces and Moments Acting on Inclined Bodies of Revolution of High Fineness Ratio. NACA RM A9I26, 1949.

13. Gowen, Forrest E., and Perkins, Edward W.: Drag of Circular Cylinders for a Wide Range of Reynolds Numbers and Mach Numbers. NACA RM A52C20, 1952.

14. Penland, Jim A.: Aerodynamic Characteristics of a Circular Cylinder at Mach Number 6.86 and Angles of Attack up to 90°. NACA RM L54A14, 1954.

15. Seaman, Donna Jean, and Dore, Frank J.: Force and Pressure Coefficients of Elliptic Cones and Cylinders in Newtonian Flow. Rep. no. 2A-7-004, Consolidated Vultee Aircraft Corp., May 16, 1952.

16. Von Kármán, Th., and Tsien, H. S.: Boundary Layer in Compressible Fluids. Jour. Aero. Sci., vol. 5, no. 6, Apr. 1938, pp. 227-232.

17. Bertram, Mitchel H.: An Approximate Method for Determining the Displacement Effects and Viscous Drag of Laminar Boundary Layers in Two-Dimensional Hypersonic Flow. NACA TN 2773, 1952.

18. Rott, Nicholas, and Crabtree, L. F.: Simplified Laminar Boundary-Layer Calculations for Bodies of Revolution and for Yawed Wings. Jour. Aero. Sci., vol. 19, no. 8, Aug. 1952, pp. 553-565.

19. Mangler, W: Boundary Layers With Symmetrical Airflow About Bodies of Revolution. Rep. no. R-30-18, Part 20, Goodyear Aircraft Corp., Mar. 6, 1946.

20. Thwaites, B.: Approximate Calculation of the Laminar Boundary Layer. Aeronautical Quarterly, vol. I, pt. III, Nov. 1949, pp. 245-280.

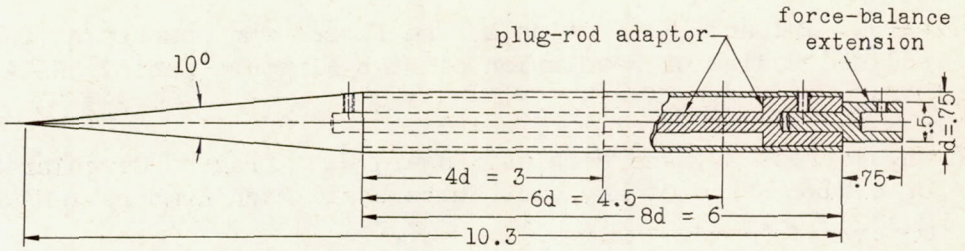

(a) 10° cone cylinder.

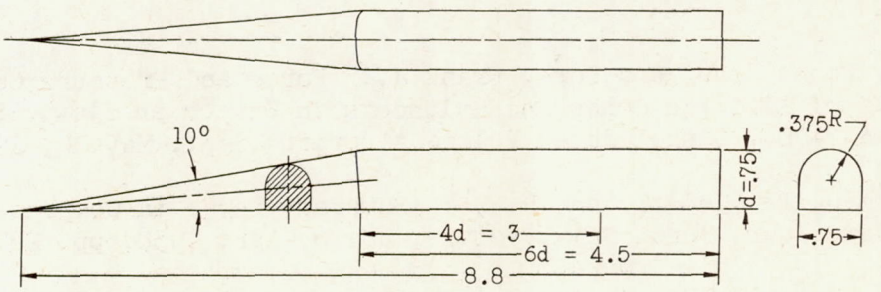

(b) D-body 1.

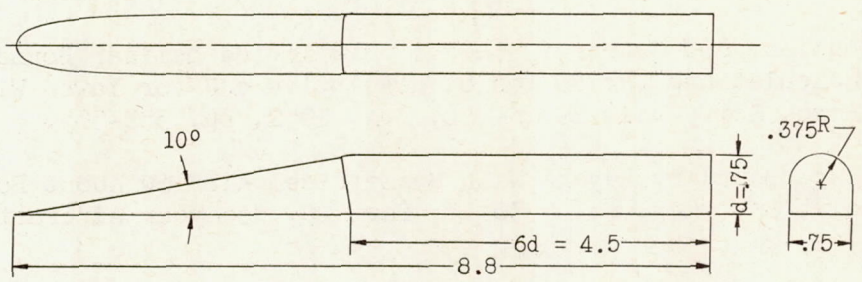

(c) D-body 2.

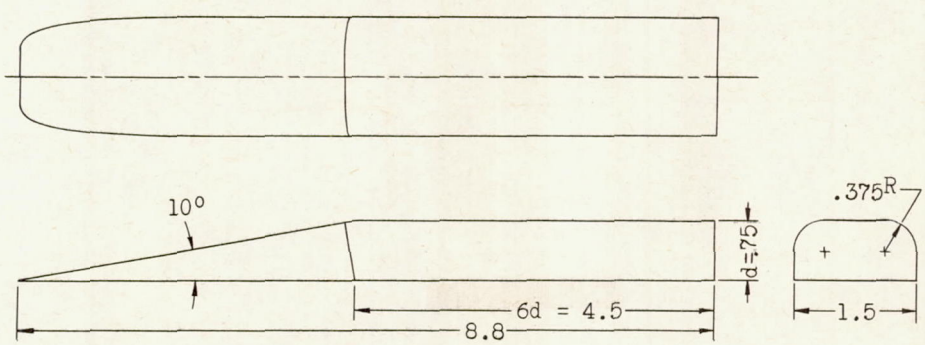

(d) D-body 3.

Figure 1.- Basic dimensions of the lifting bodies. All dimensions are in inches.

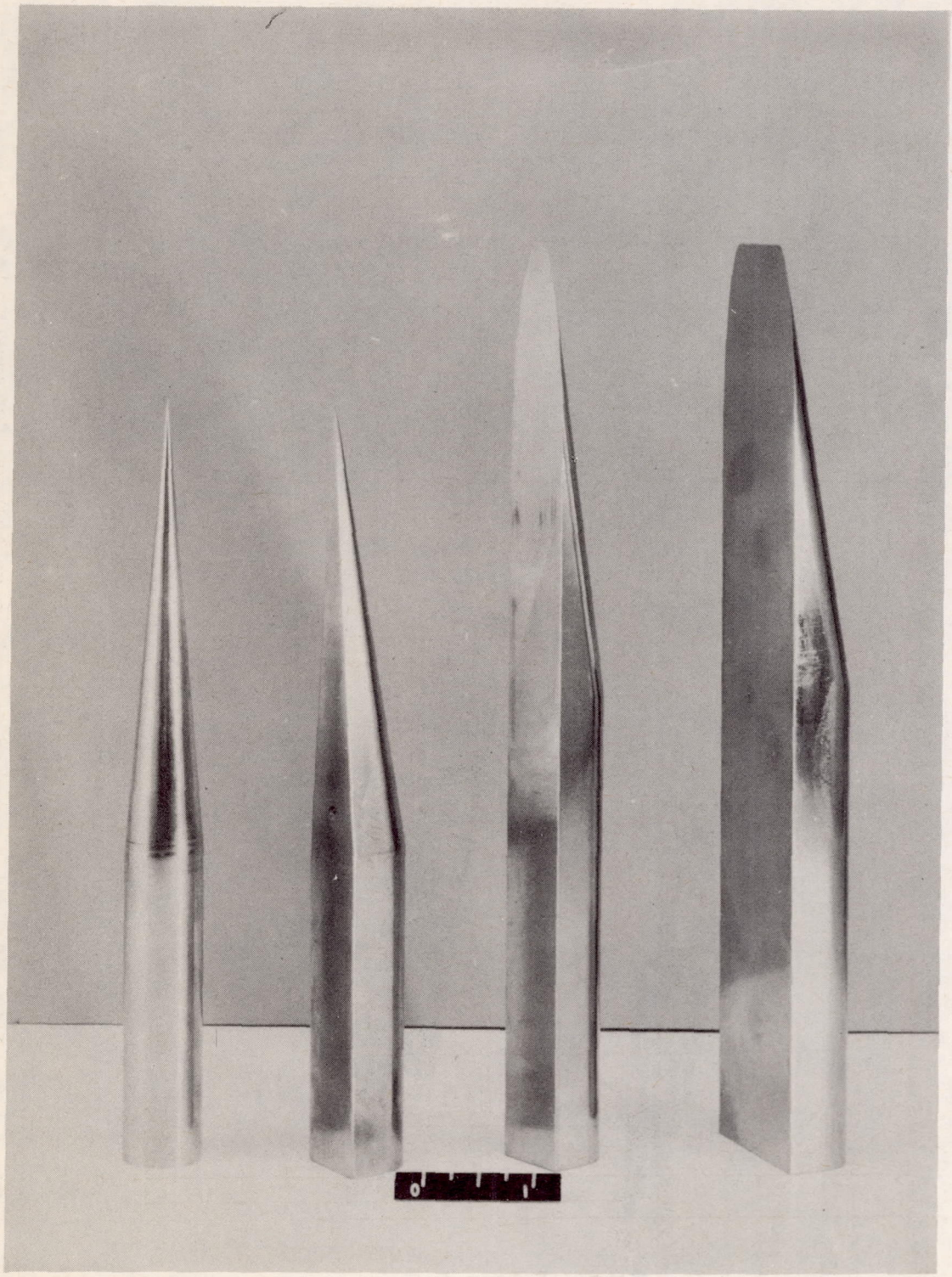

L-79802

Figure 2.- The lifting bodies appear from left to right as follows: 10° cone cylinder with a 4-diameter afterbody, D-body 1 with a 4-diameter afterbody, D-body 2, and D-body 3.

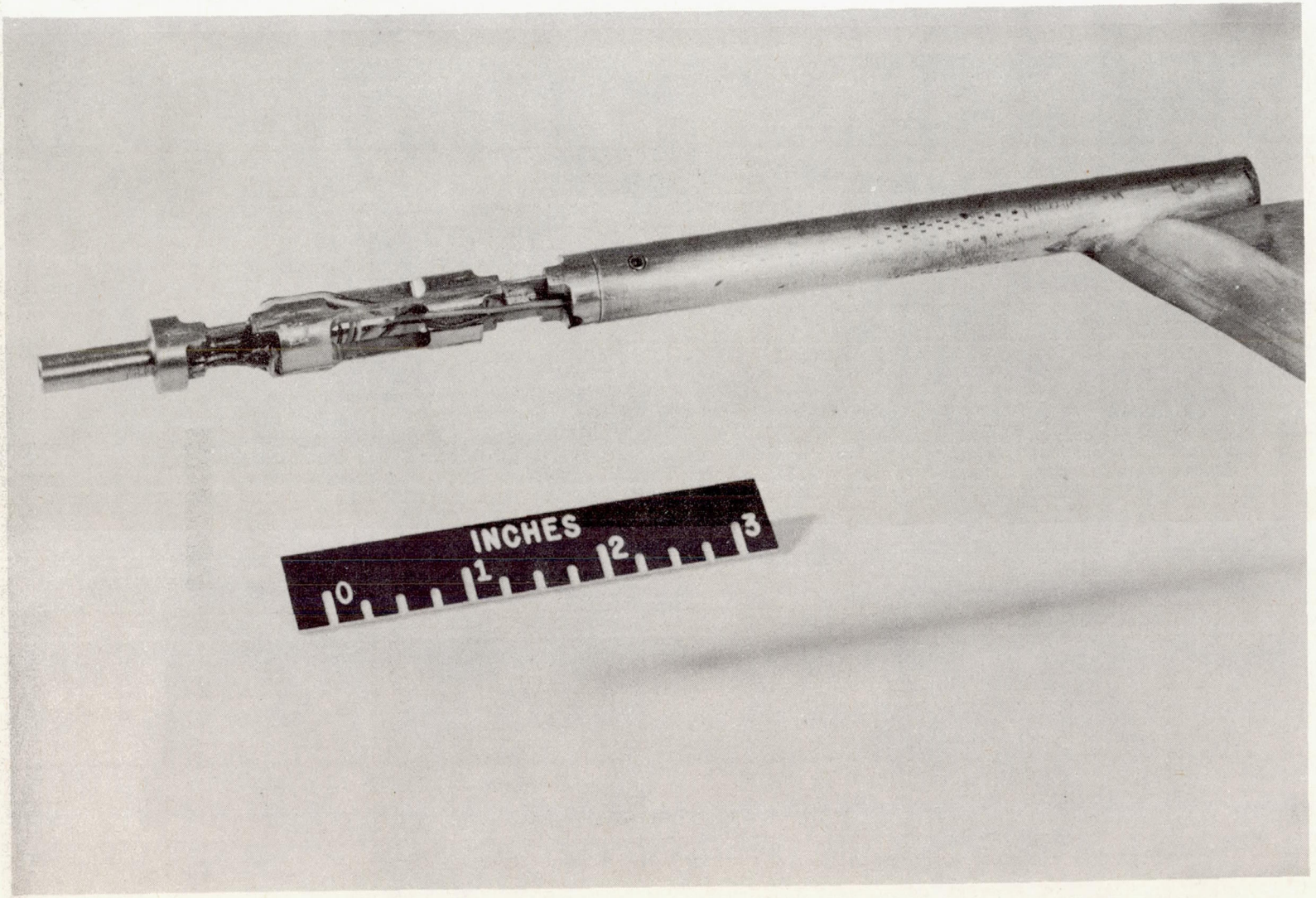

L-80926

Figure 3.- Internal, sting-mounted, strain-gage balance for measuring pitching moment.

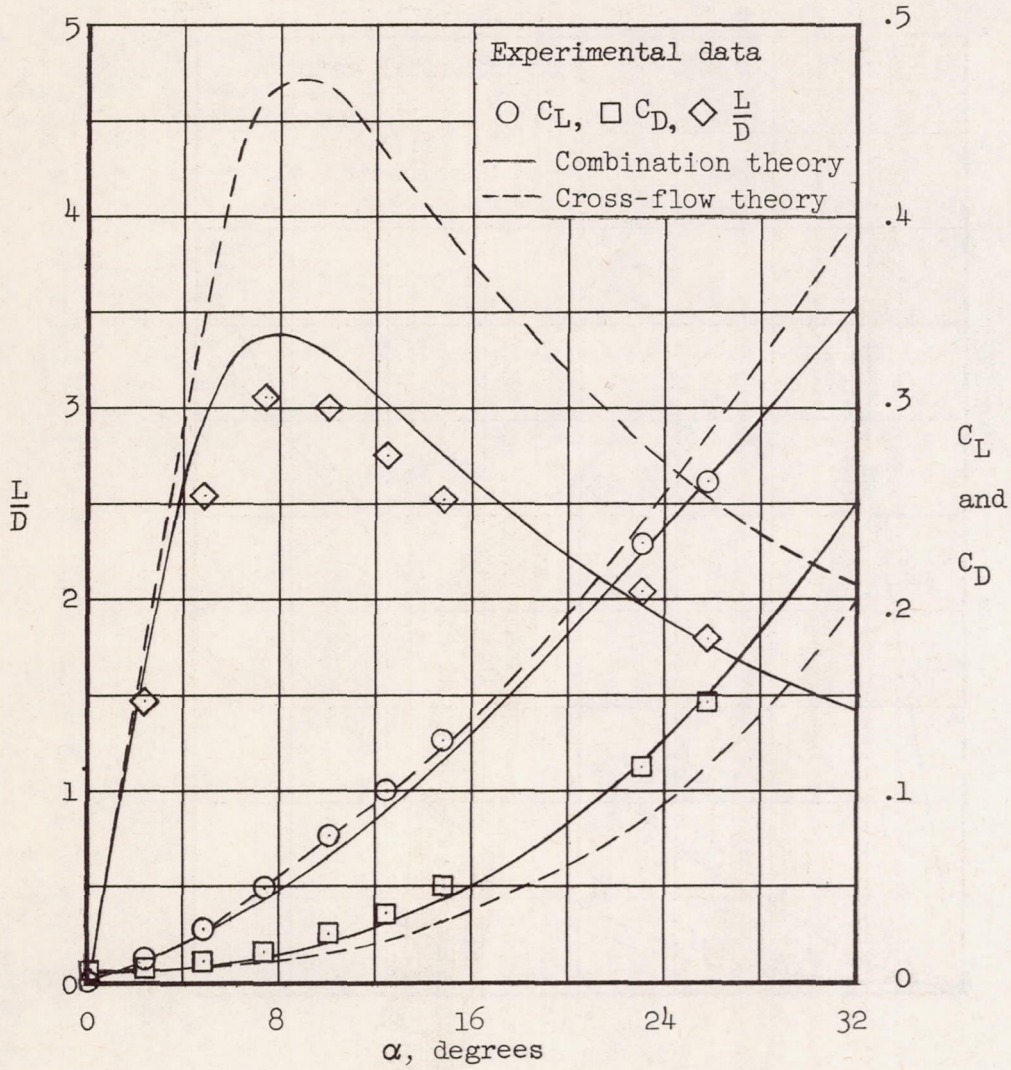

(a) 4d.

Figure 4.- Variation with angle of attack of C_L, C_D, and L/D for a 10° cone cylinder with afterbody lengths of 4, 6, and 8 diameters at M = 6.86.

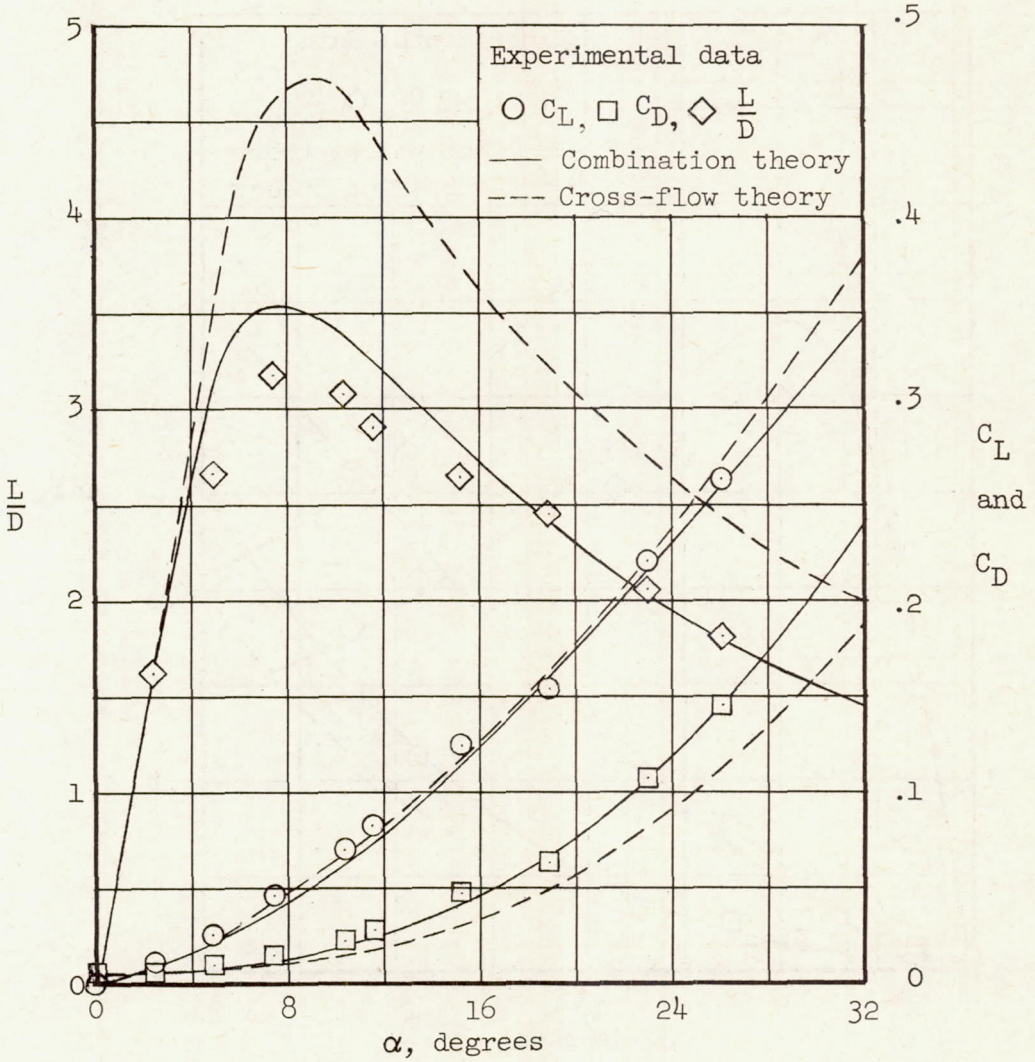

(b) 6d.

Figure 4.- Continued.

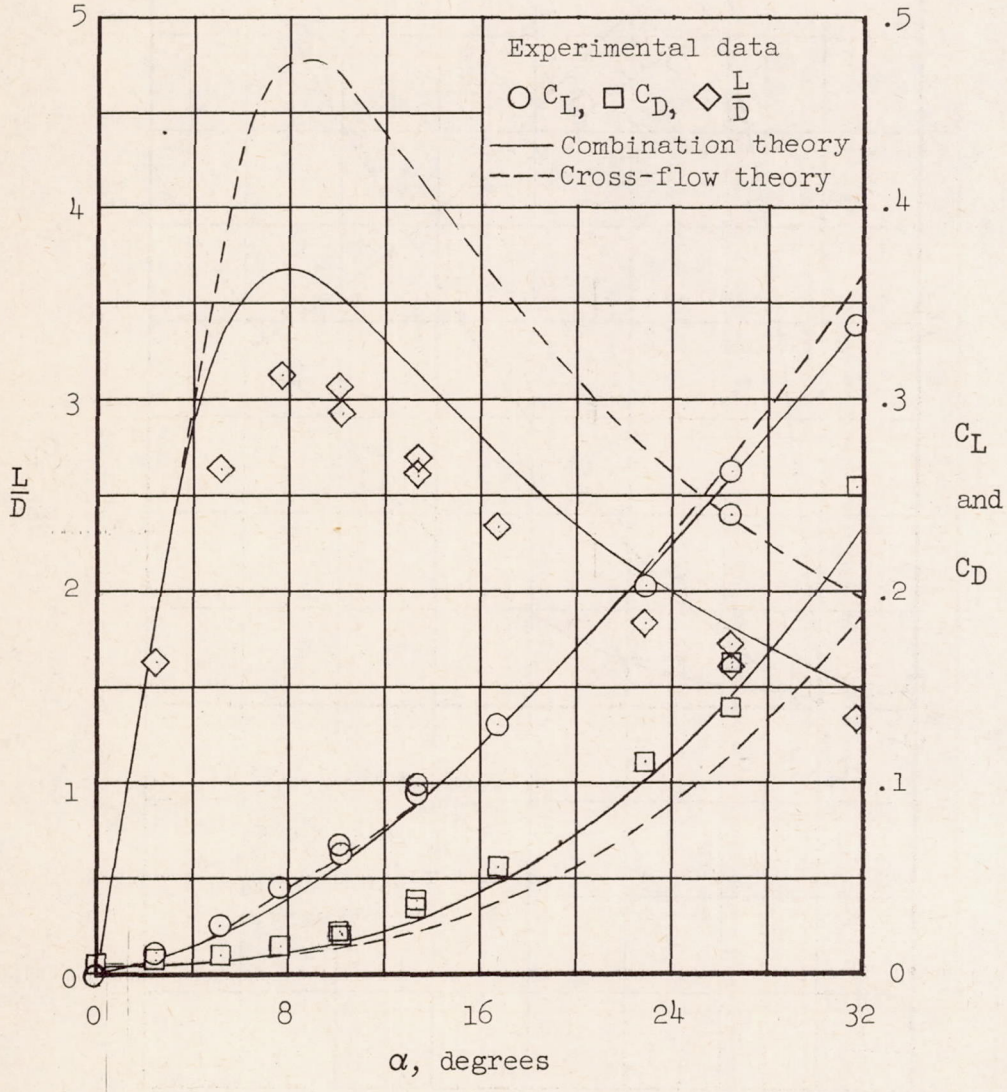

(c) 8d.

Figure 4.- Concluded.

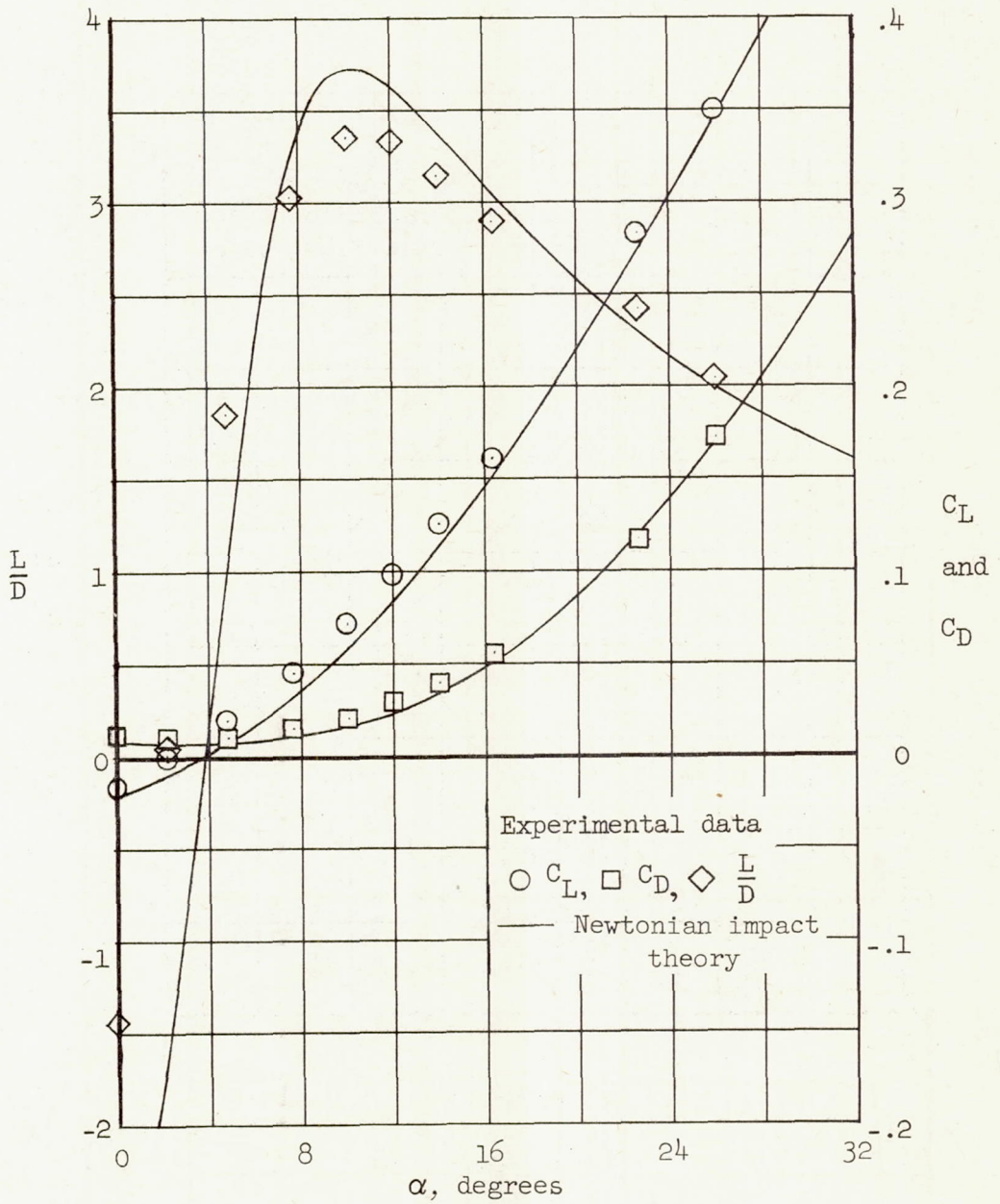

(a) 4d.

Figure 5.- Variation with angle of attack of C_L, C_D, and L/D for D-body 1 with afterbody lengths of 4 and 6 diameters at M = 6.86.

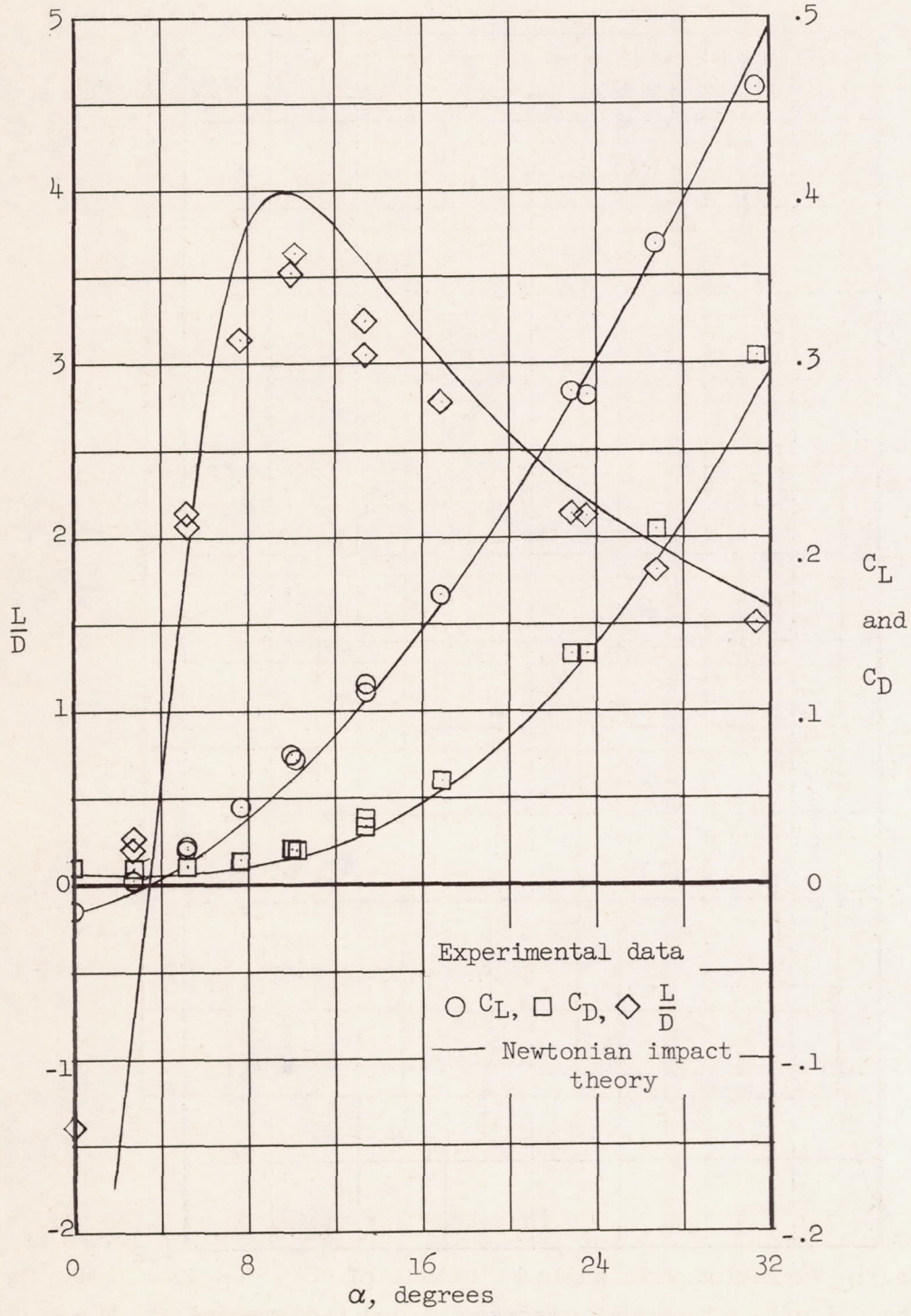

(b) 6d.

Figure 5.- Concluded.

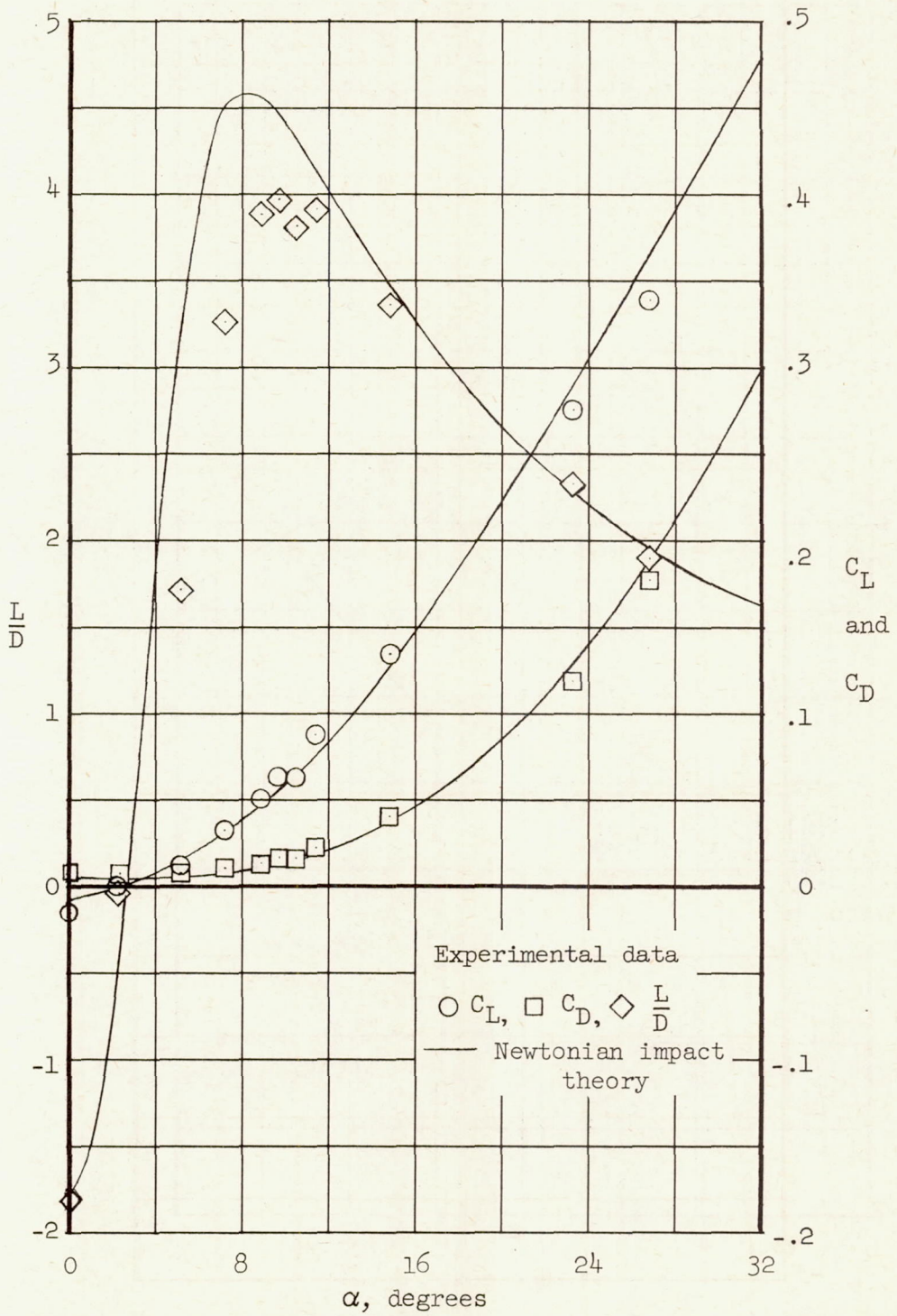

Figure 6.- Variation with angle of attack of C_L, C_D, and L/D for D-body 2 at M = 6.86.

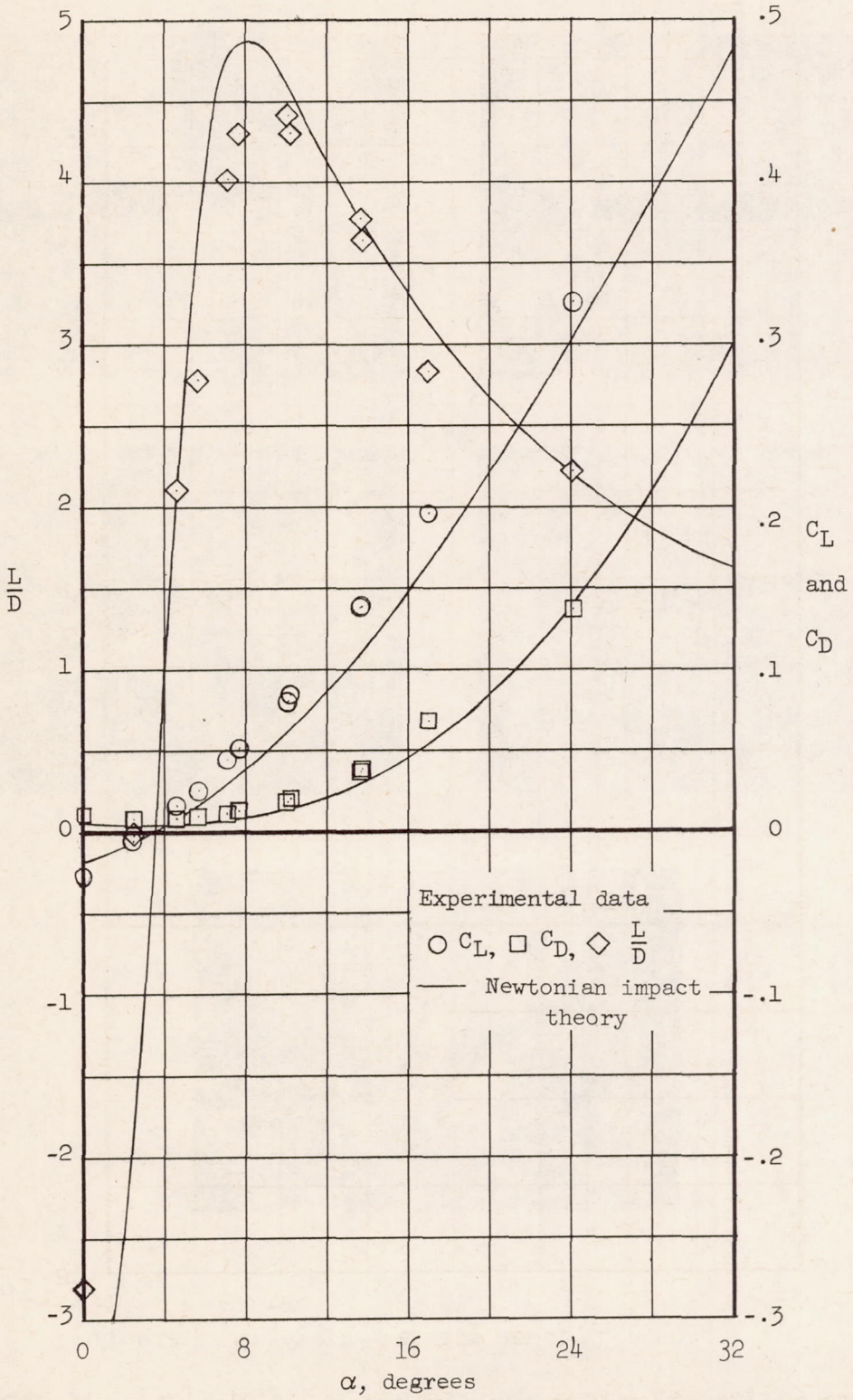

Figure 7.- Variation with angle of attack of C_L, C_D, and L/D for D-body 3 at M = 6.86.

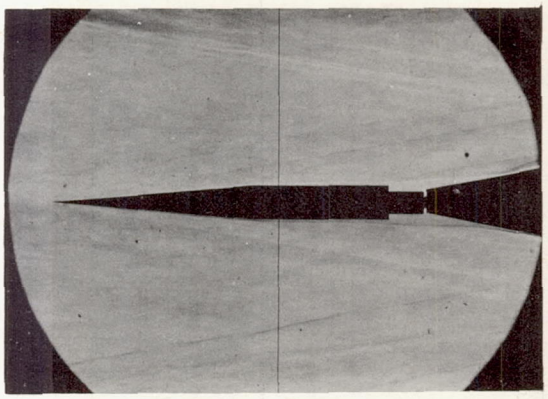

$\alpha = 0^\circ$

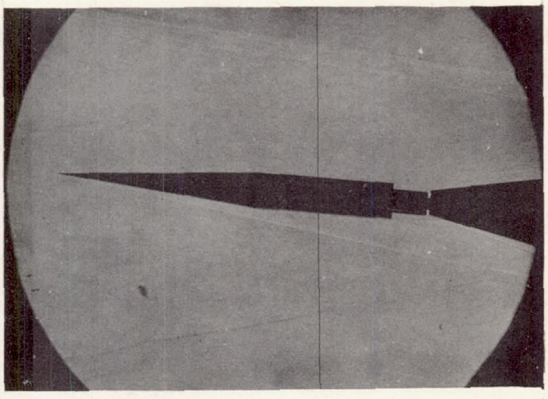

$\alpha = 4.9^\circ$

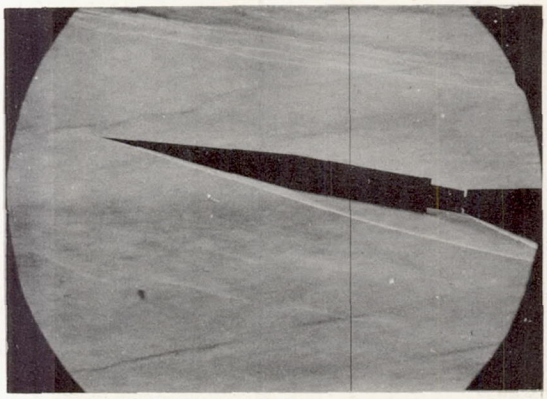

$\alpha = 10.1^\circ$

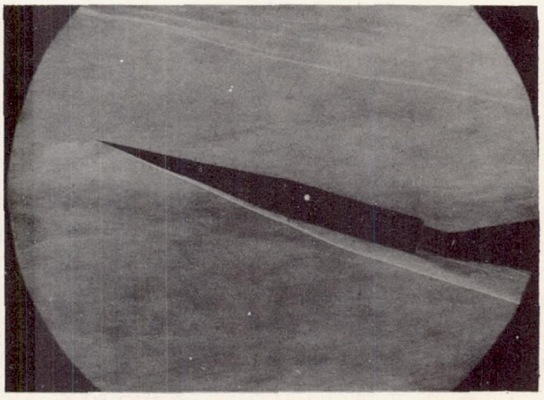

$\alpha = 14.8^\circ$

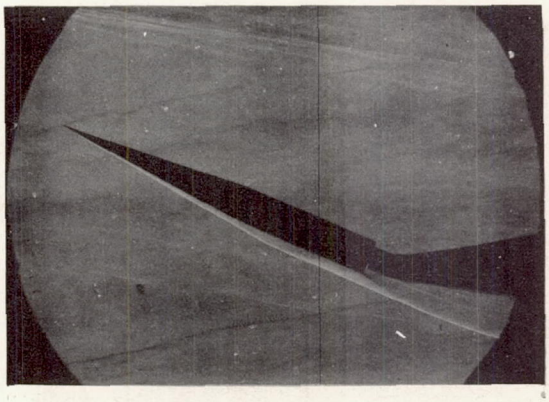

$\alpha = 23.1^\circ$

L-83339

(a) 10° cone cylinder with a 4-diameter afterbody.

Figure 8.- Typical schlieren pictures of the lifting bodies at various angles of attack at $M = 6.86$.

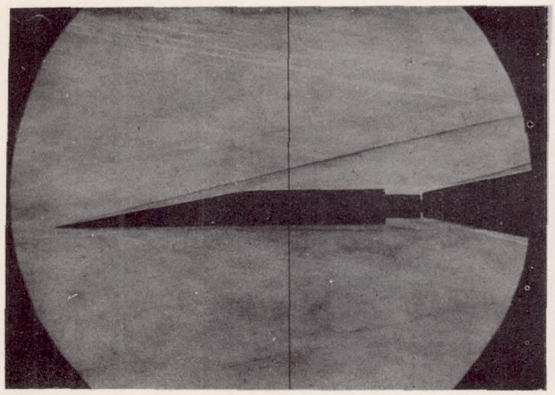

$\alpha = 0^\circ$

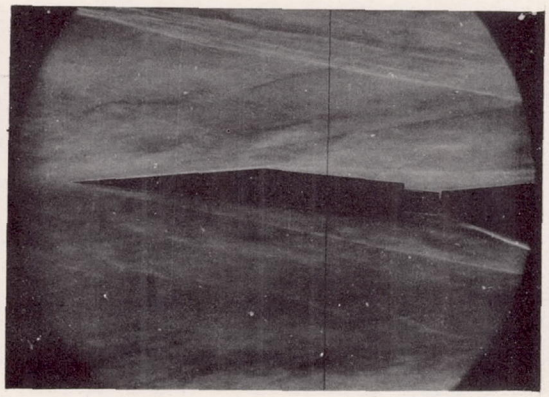

$\alpha = 4.8^\circ$

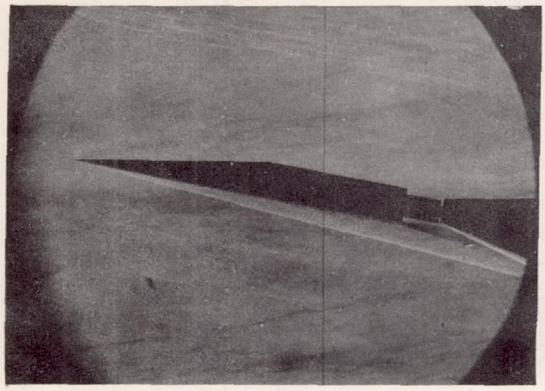

$\alpha = 10.1^\circ$

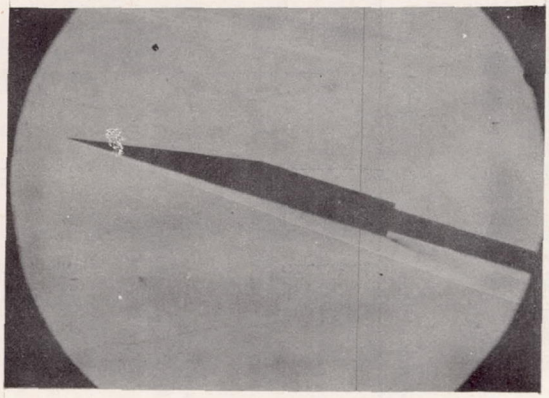

$\alpha = 15^\circ$

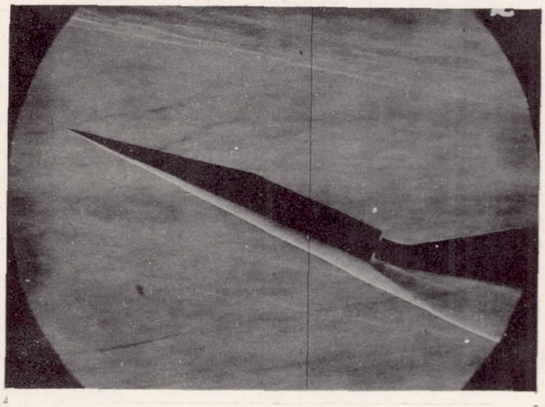

$\alpha = 22.6^\circ$

L-83340

(b) D-body 1 with a 4-diameter afterbody.

Figure 8.- Concluded.

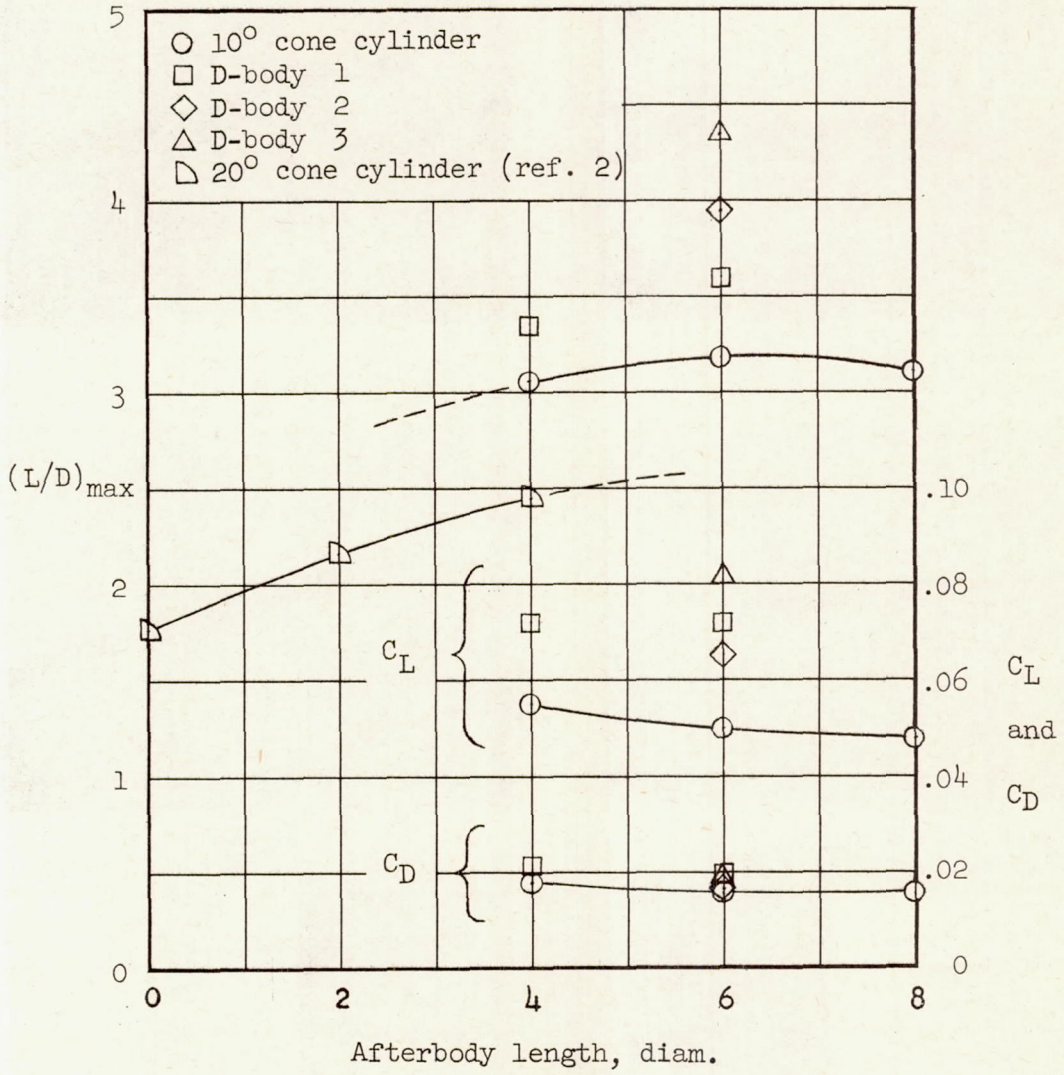

Figure 9.- Variation with afterbody length of the maximum lift-drag ratio and the lift and drag coefficients at the angle of attack corresponding to the maximum lift-drag ratio for the lifting bodies at M = 6.86.

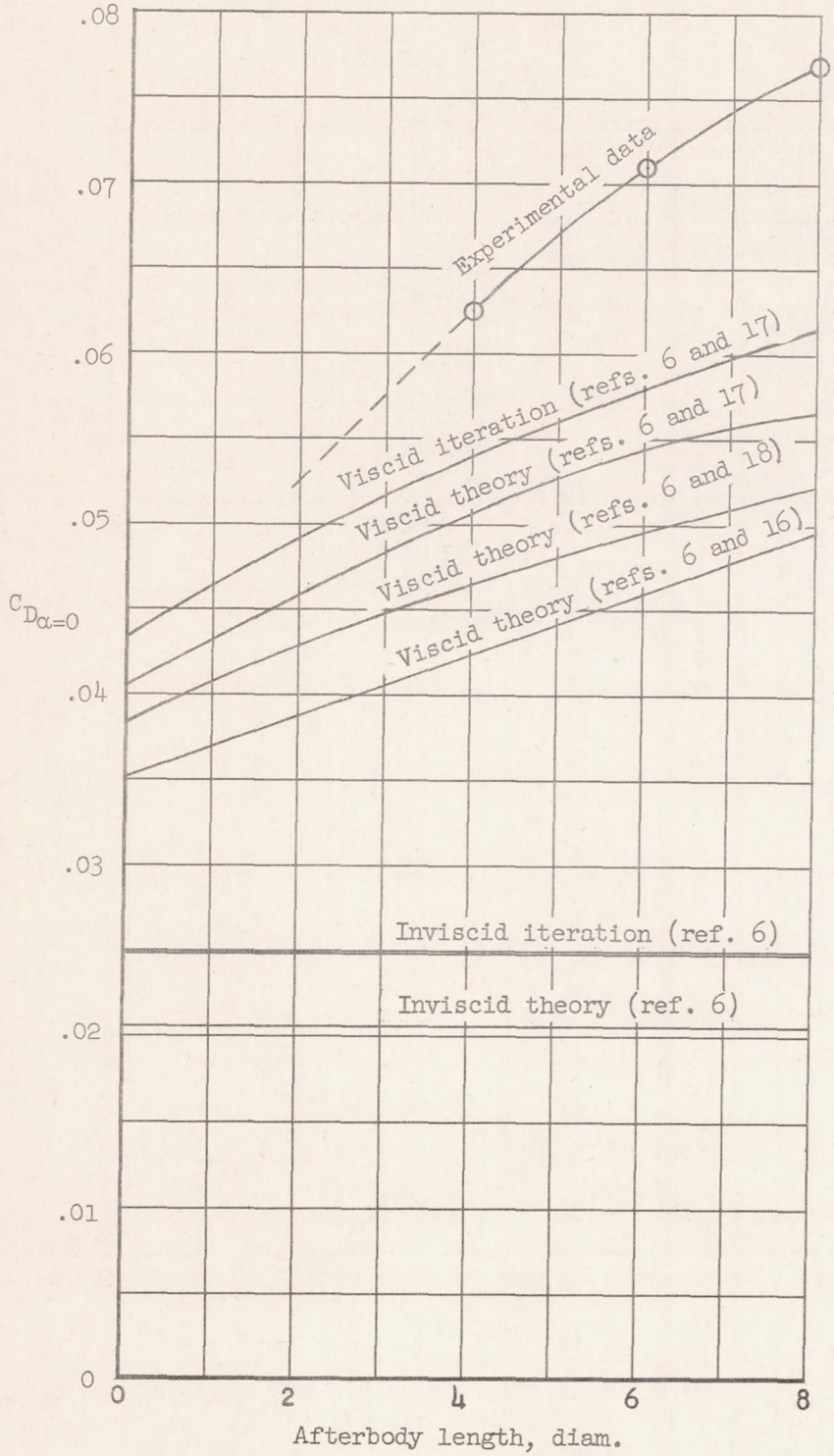

Figure 10.- Variation of the experimental and theoretical drag coefficients (based on base area) at zero angle of attack with afterbody length for 10° cone cylinders at M = 6.86.

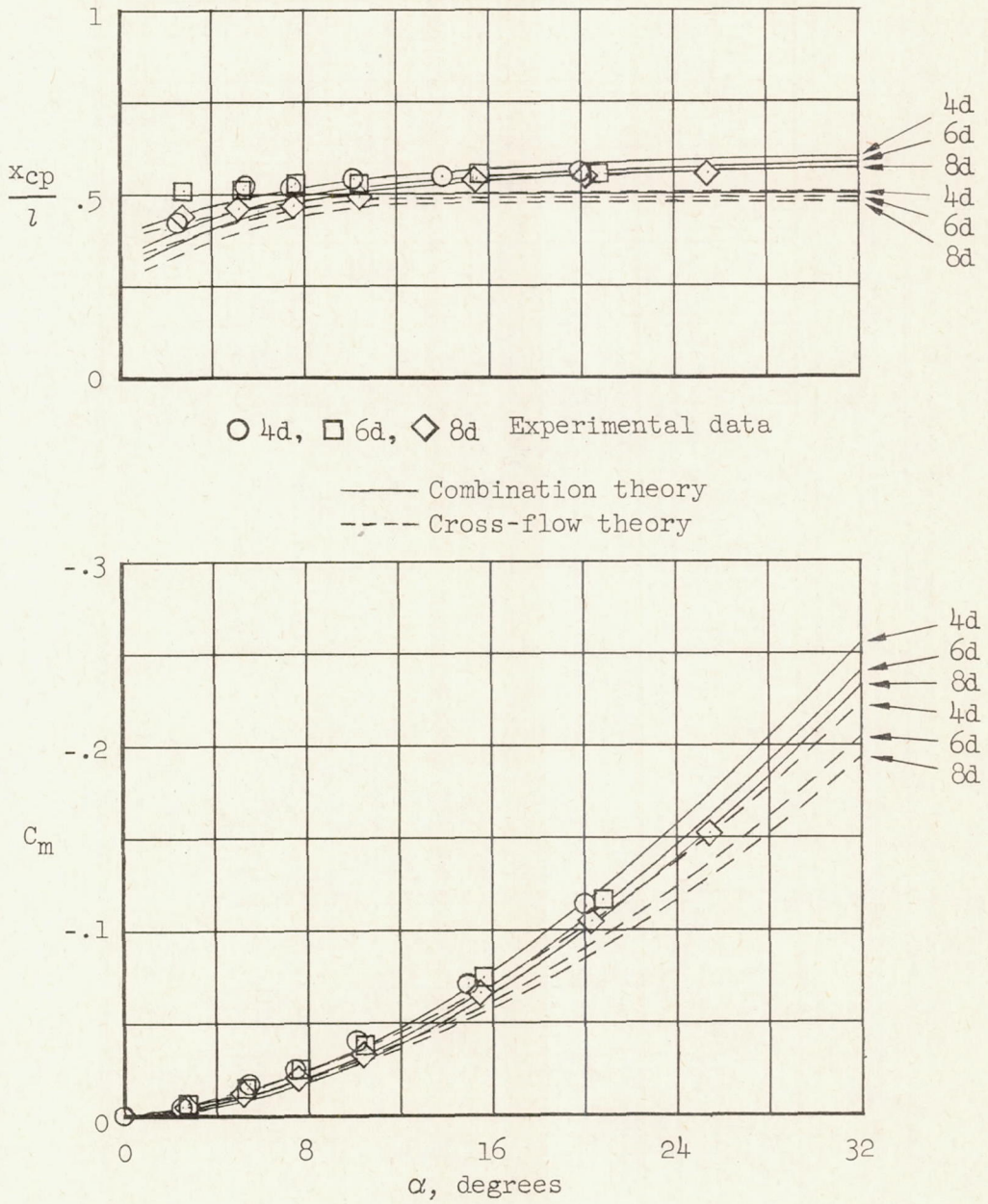

Figure 11.- Variation with angle of attack of the pitching-moment coefficient (moments are taken about the nose of the model) and the center-of-pressure location (distance from nose in body lengths) for a 10° cone cylinder with afterbody lengths of 4, 6, and 8 diameters at M = 6.86.

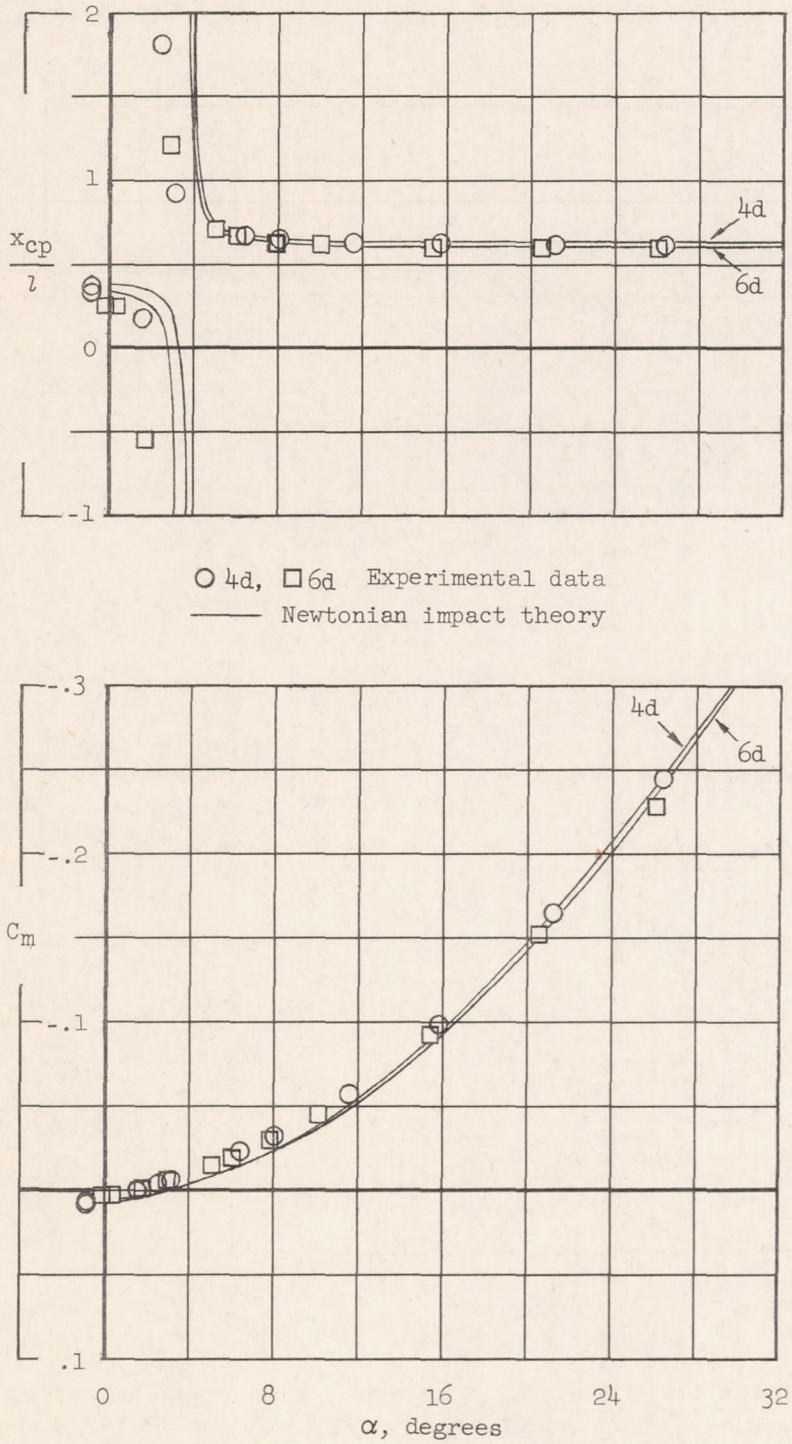

Figure 12.- Variation with angle of attack of the pitching-moment coefficient (moments are taken about the nose of the model) and center-of-pressure location (distance from nose in body lengths) for D-body 1 with afterbody lengths of 4 and 6 diameters at M = 6.86.